

Impedance/Dielectric Spectroscopy of Electroceramics in the Nanograin Regime

by

N.J. Kidner, B. J. Ingram, Z.J. Homrighaus, T.O. Mason
Department of Materials Science and Engineering and Materials Research Center
Northwestern University
Evanston, IL 60208 USA

and

E.J. Garboczi
Building and Fire Research Laboratory
National Institute of Standards and Technology
Gaithersburg, MD 20899 USA

Reprinted from Proceedings from the Solid-State Ionics 2002, Materials Research Society 2002 Fall Meeting, Volume 756, Boston, MA, EE4.6.1-12 pp., 2003.

NOTE: This paper is a contribution of the National Institute of Standards and Technology and is not subject to copyright.

NIST

National Institute of Standards and Technology
Technology Administration, U.S. Department of Commerce

Impedance/Dielectric Spectroscopy of Electroceramics in the Nanograin Regime

N. J. Kidner, B. J. Ingram, Z. J. Homrighaus, T. O. Mason, and E. J. Garboczi¹

Department of Materials Science and Engineering and Materials Research Center, Northwestern University, Evanston, IL 60208, U.S.A.

¹Materials and Construction Research, Building and Fire Research Laboratory, National Institute of Standards and Technology, Gaithersburg, MD 20899, U. S. A.

ABSTRACT

In the microcrystalline regime, the behavior of grain boundary-controlled electroceramics is well described by the “brick layer model” (BLM). In the nanocrystalline regime, however, grain boundary layers can represent a significant volume fraction of the overall microstructure and simple layer models are no longer valid. This work describes the development of a pixel-based finite-difference approach to treat a “nested cube model” (NCM), which more accurately calculates the current distribution in polycrystalline ceramics when grain core and grain boundary dimensions become comparable. Furthermore, the NCM approaches layer model behavior as the volume fraction of grain cores approaches unity (thin boundary layers) and it matches standard effective medium treatments as the volume fraction of grain cores approaches zero. Therefore, the NCM can model electroceramic behavior at all grain sizes, from nanoscale to microscale. It can also be modified to handle multi-layer grain boundaries and property gradient effects (e.g., due to space charge regions).

INTRODUCTION

There are a number of existing and proposed applications of electroceramics in nanocrystalline form, including batteries, fuel cells, gas separation membranes, solar cells, etc. [1] Nanoceramics are utilized as chemical catalysts and as chemical sensors. Their microcrystalline counterparts are often used as active electrical devices (e.g., varistors and thermistors). In certain cases, like the latter, grain boundaries are necessary to impart the required electro-active or thermo-active responses. In other cases, grain boundaries act as undesirable barriers limiting transport (e.g., in ionic conductors). In still others, boundaries between dissimilar ceramics can impart enhanced ion transport due to high mobility space charge regions (e.g., in “dispersed ionic conductors”) [2,3]. Given the high surface-to-volume ratios in nanoceramics, grain boundaries can be expected to exert greater influence over electrical/dielectric properties than in conventional microcrystalline ceramics.

There are several problems with existing grain boundary layer models (see below) insofar as describing the electrical/dielectric response of nanoceramics is concerned. First, in the nanograin regime, boundary layers such as space-charge regions or local oxidation layers can represent a significant volume fraction of the overall microstructure (see Figure 1). Conventional layer models, such as the “brick layer model” (BLM), are hardly adequate for such a situation. Second, as pointed out by Maier [4], there can be differential transport coefficients parallel vs. perpendicular to the grain boundaries. Finally, space charge regions represent spatially varying electrical properties, which are not consistent with the simple property step functions assumed in most layer models.

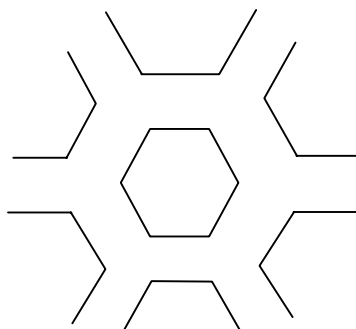


Figure 1. Schematic of nanostructure with a significant grain boundary layer

The BLM was first conceived 25 years ago by Beekmans and Heyne [5], although Burggraaf and co-workers are credited with coining the “brick layer” name [6,7]. The microstructural picture is represented by Figure 2. The simplest form of the BLM, which we refer to as the series-BLM (S-BLM), ignores the side-wall contributions (on the left) and considers only the serial connections of grain cores and capping grain boundary layers (on the right). The corresponding equivalent circuit is shown in Figure 3a, where the open box represents the equivalent circuit ($R_{gc}C_{gc}$) of the grain cores and the shaded box represents the equivalent circuit ($R_{gb}C_{gb}$) of the grain boundaries. Using the notation of Boukamp [8], this series combination of two (RC) parallel circuits can be represented as $(R_{gb}C_{gb})(R_{gc}C_{gc})$. This model is quite appropriate for thin, continuous, and highly resistive second phase films such as siliceous layers in low purity, microcrystalline ionic conductors [9].

The major deficiency of the S-BLM, ignoring side-wall contributions, was addressed by Näfe [10], who developed a series/parallel BLM (SP-BLM) by connecting the central grain core/grain boundary serial path of Figure 2 (on the right) in parallel with the side-wall grain boundary path (on the left). The corresponding equivalent circuit is shown in Figure 3b. We recently applied the SP-BLM to the analysis of nanoceramic impedance/dielectric spectra [11].

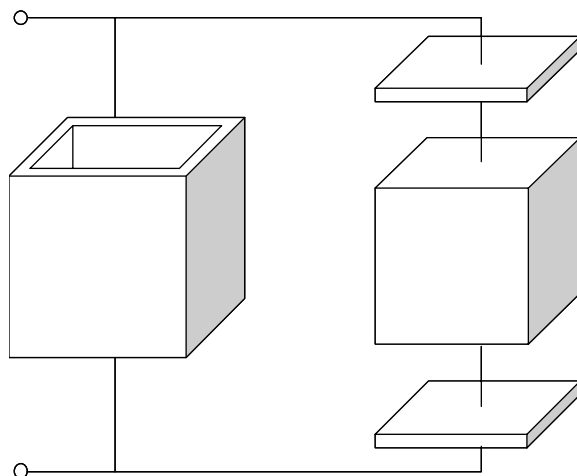


Figure 2. The brick layer model with series/parallel connectivity.

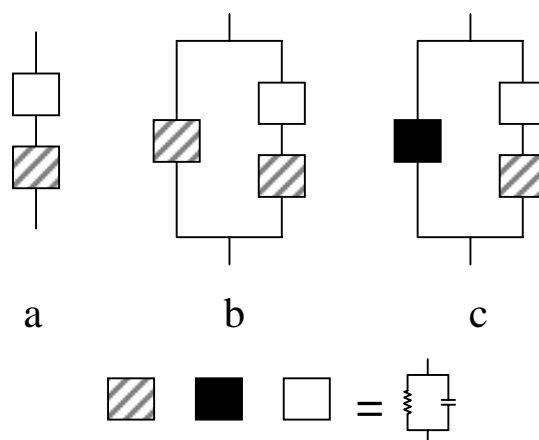


Figure 3. Equivalent circuit representations for a) the series brick layer model (S-BLM), b) the series/parallel BLM (SP-BLM), and c) the SP-BLM with different electrical properties parallel vs. perpendicular to the grain boundary.

A modified form, which we refer to as the SP'-BLM, was developed by Maier and coworkers [3,12] to allow for differential electrical conductivity perpendicular vs. parallel to the grain boundary. The SP'-BLM equivalent circuit model is shown in Figure 3c.

A limitation common to both SP-BLM and SP'-BLM models is that current flow is restricted to either the central core (series) path or the outer (parallel) path, which is clearly not the case in an actual nanostructure (see Figure 1). Bonanos et al. [9] commented that the SP-BLM “is valid at high or low conductivity ratios...” but had “reservations about the use of this model over the entire σ_{gc}/σ_{gb} range, since it is not clear how, when $\sigma_{gb} \sim \sigma_{gc}$, this assumption that the current flows via two separate mechanisms can be tenable.” Based upon comparison with the Maxwell-Wagner/Hashin-Shtrikman effective medium theory, which sets the absolute upper and lower limits of conductivity for isotropic two-phase composites, McLachlan et al. [13] concluded that “...where it (the SP-BLM) lies outside the MW-HS limits (which it does at most intermediate grain core volume fractions) it is fundamentally wrong.”

Effective medium theory (EMT) has also been applied to the complex impedance/ dielectric response of electroceramics. EMT models obviate the limitations of the layer models by taking into account real current distributions in heterogeneous media. They therefore provide important benchmarks against which to compare microstructurally-based models.

As early as 1914, Wagner [14] showed that Maxwell’s equation for DC conductivity [15] also worked for the complex conductivity. A MW medium can be visualized as built up from a space-filling array of coated spheres, as in Figure 4, with each sphere surrounded by a mixture of the two components having the mean or effective property value of the medium. As pointed out by McLachlan et al. [13], the MW model is equivalent to the Hashin-Shtrikman upper and lower bounds for conductivity of an isotropic two-phase mixture [16] and the well known Clausius-Mossoti equation for dielectrics. In the limit that the volume fraction of the continuous (matrix) phase becomes small (thin boundary layers), we showed that the impedance/dielectric response becomes indistinguishable from the brick layer models [13]. Thin coatings, whether insulating

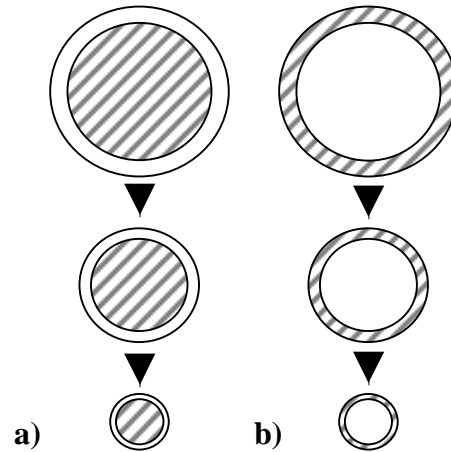


Figure 4. The basic building blocks for the Maxwell-Wagner/Hashin Shtrikman effective media, with either a) conductive coatings or b) insulating coating.

or conductive relative to the cores, behave identically regardless of the grain morphology (i.e., spheres vs. cubic “bricks”). Finite element analyses on “real” 2-D microstructures agreed well with BLM predictions unless grain shape became highly distorted or a bimodal distribution of grain sizes was present [17-19]. This means that simplified morphologies, whether spherical (i.e., the various EMT models) or cubic (e.g., the nested-cube model below), stand a very good chance of accurately describing the impedance/dielectric response of nanostructures with equiaxed, mono-sized grains.

The range of minority phase volume fractions over which the MW-HS model is believed to be valid is $0 \leq \phi \leq 0.3$ [9]. We are interested in developing a model capable of traversing the entire range of grain core volume fraction from 0 (nanoscale) to 1 (microscale), assuming nanometer scale boundary layers, e.g., consistent with space charge layers in electroceramics. One model pertinent to the present work is that of Zuzovsky and Brenner [20]. The Zuzovsky-Brenner Model (ZBM) consists of a cubic array of second phase spherical particles suspended in a continuous matrix phase, the unit cell of which is shown in Figure 5a. This model is perhaps the

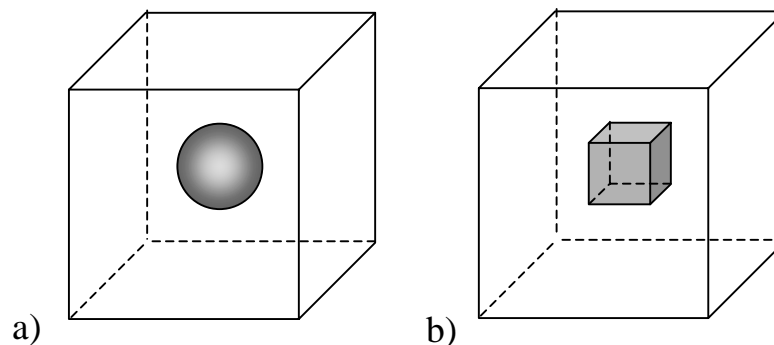


Figure 5. Unit cells of the a) Zuzovsky/Brenner model, with spherical second phase particles (grain cores) on a simple cubic lattice and b) the nested cube model, with cubic second phase particles (grain cores) on a simple cubic lattice.

most representative of the situation in nanoceramics with relatively thick grain boundary layers; grain core morphology will most likely *not* maintain overall grain shape due to smearing/rounding of boundary layers (e.g., space charge regions, see figure 1). The problem with the ZBM is that a percolation threshold (grain core-to-grain core) is reached at a grain core volume fraction of 0.52.

The present work reports the development of an analogous nested-cube model or NCM, the unit cell of which is shown in Figure 5b. The NCM has no percolation threshold, and is capable of describing impedance/dielectric behavior over the entire range of grain core fractions, from small values (where it matches ZBM behavior and also agrees with MW-HS model results) to large values (where it matches the brick layer model results). As we will show, the NCM also has potential for describing multi-layer grain boundary structures and property gradients at grain boundaries (e.g., in space charge regions).

EXPERIMENTAL DETAILS

The nested cube model is not tractable analytically. A FORTRAN-77 finite-difference numerical program, **ac3d.f**, was therefore modified to carry out pixel-based computer calculations at finite frequencies. This program, developed at NIST, can be accessed at <http://ciks.cbt.nist.gov/monograph/>, Chapter 2, along with a manual in HTML format [21]. The program was designed to compute the electrical properties of random materials whose microstructure can be represented by a 3-D digital image. It can also be used to simulate non-random, but analytically intractable geometries, as in the present work. A system size of between 20^3 and 80^3 pixels was employed to represent the 3-D structure of the NC model in Fig. 5b. Depending on the grain size, pixels are either grain core or grain boundary (for a single grain boundary layer). In the computation process, a finite-difference node is set up in the middle of each pixel. As part of the computation, bonds are assigned between each pair of nodes reflecting the (RC) values assigned to each pixel. A conjugate gradient method is then used to solve Laplace's equation at each frequency to give the complex conductivity of the microstructure. Real and imaginary conductivities are then converted to impedance and modulus quantities via standard equations.

To generate the periodic simple cubic lattice of the NCM, it is necessary to add a shell of imaginary states around the main system to maintain the periodic boundary conditions. For a given grain core volume fraction, the system size is varied to assess the effect of spatial resolution. A plot of conductivity vs. $1/N$ (where N is the number of pixels) is extrapolated to give the conductivity at $1/N \rightarrow 0$. Computing time restricted system size to below 100^3 pixels.

The NCM was compared to EMT models (MW-HS) and the ZBM at small-to-intermediate grain core volume fractions, and to the S-BLM and SP-BLM models at intermediate-to-large grain core volume fractions. Unlike the NCM, analytical equations exist for each of these models, which could be expressed in terms of complex conductivities, $\sigma^* = \sigma_r + i\sigma_i$, involving both real (σ_r) and imaginary (σ_i) components. Standard equations were employed in each case to convert to impedance and modulus formats. We also considered Bode plots (log-log plots of real and imaginary impedance or capacitance vs. frequency).

RESULTS AND DISCUSSION

First to be considered is the case of large grain core volume fraction, i.e., thin grain boundary layers. Figure 6 shows a Nyquist (impedance or Z-plane) plot of NCM results vs. the two brick layer models. The ZBM is not valid at this volume fraction of grain cores (0.927), since this is above the percolation threshold of the ZBM (0.52). The ratio of grain boundary-to-grain core conductivity (σ_{gb}/σ_{gc}) was set at 0.1 and the dielectric constants were the same ($\epsilon_{gb}=\epsilon_{gc}$). The NCM is in good agreement with both the S-BLM and the SP-BLM, as also seen in modulus and Bode plots (not shown). This is to be expected, since the grain boundary layers are quite thin at this value of grain core volume fraction; D/d , the ratio of grain core dimension to grain boundary thickness is approximately 39. The NCM picture at large grain core volume fraction closely resembles that of the boundary layer models, especially the SP-BLM.

At the other end of the relative size spectrum, Z-plane results for a small grain core volume fraction (0.162) are shown in Figure 7. The ratio of grain core-to-grain boundary dimension is now $D/d\sim 1.20$. For the calculations, the ratios of grain boundary-to-grain core properties were set at $\sigma_{gb}/\sigma_{gc}=0.10$ and $\epsilon_{gb}/\epsilon_{gc}=10$, respectively. The NCM results are seen to approach the MW-HS predictions, which is important, since realistic models must agree with EMT predictions at small volume fractions. This agreement was also observed in Modulus and Bode plots (not shown). There is also reasonable agreement between the NCM results and ZBM predictions. Some differences can be anticipated based on the difference in grain core morphologies (see Figure 5). If we consider the dilute limit ($\phi < 0.1$), the conductivity of a composite (σ) relative to that of the matrix (σ_m) should vary with the volume fraction of highly conductive second phase particles according to [22]:

$$(\sigma/\sigma_m) = 1 + [\sigma]_{\infty} \phi \quad (1)$$

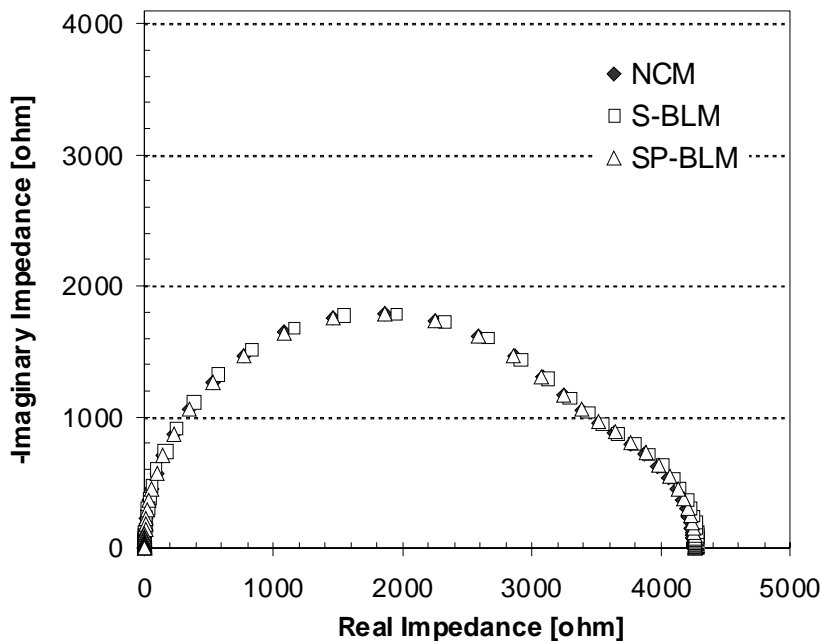


Figure 6. Simulated impedance response for various models assuming $\sigma_{gb}/\sigma_{gc} = 0.1$, $\epsilon_{gb}=\epsilon_{gc}$, and a volume fraction of 0.927 for grain cores. See text for code to models.

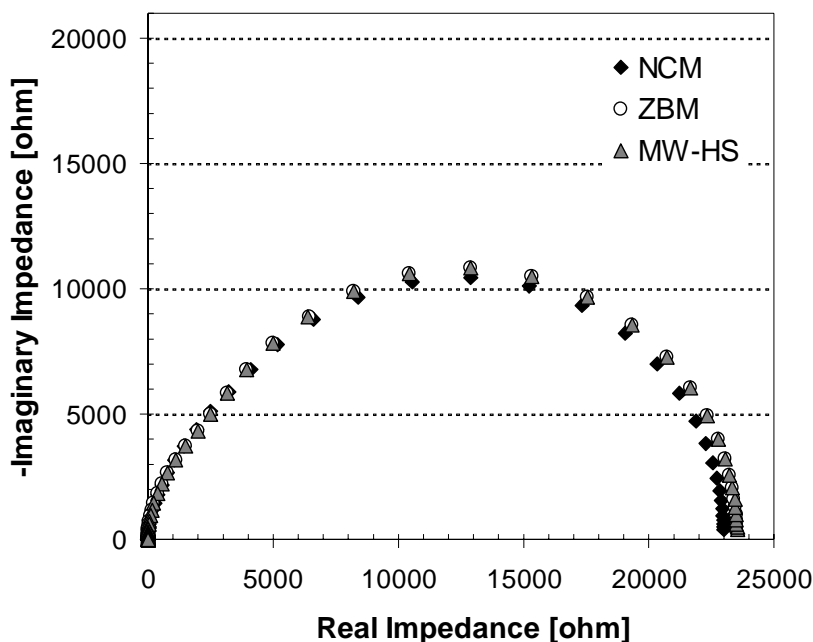


Figure 7. Simulated impedance response for various models assuming $\sigma_{gb}/\sigma_{gc} = 0.1$, $\epsilon_{gb}/\epsilon_{gc}=10$, and a volume fraction of 0.162 for grain cores. See text for code to models.

where $[\sigma]_{\infty}$ is the “intrinsic conductivity” of the conducting particles, each shape having a characteristic value. It has been established that the intrinsic conductivity of a conductive cube is 3.4 whereas that of a conductive sphere is 3.0 [22]. Therefore, it is not surprising to see some differences, but otherwise close similarity between the two models. In the intrinsic range ($\phi < 0.1$) we found that both the ZBM and NCM agreed well with the MW-HS model.

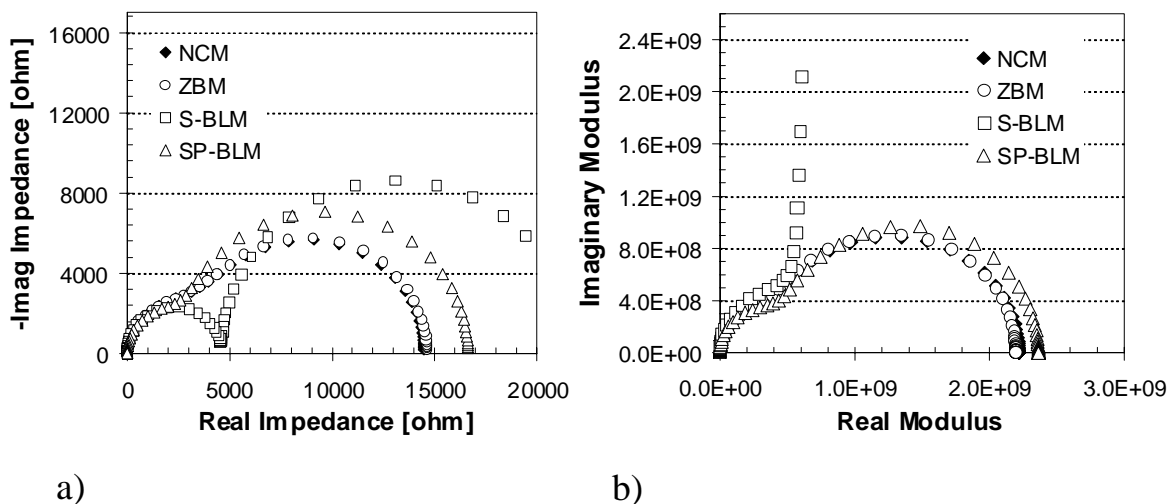


Figure 8. Simulated a) impedance and b) modulus response for various models assuming $\sigma_{gb}/\sigma_{gc} = 0.1$, $\epsilon_{gb}/\epsilon_{gc} = 100$, and a volume fraction of 0.385 for grain cores. See text for code to models.

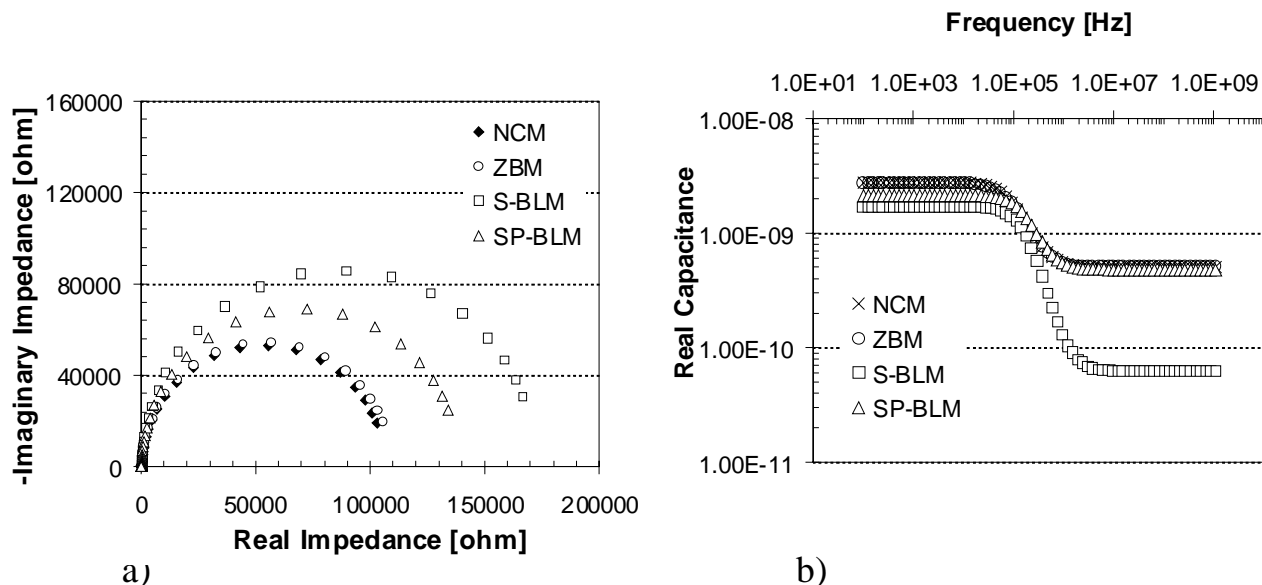


Figure 9. Simulated a) impedance and b) capacitance Bode response for various models assuming $\sigma_{gb}/\sigma_{gc} = 0.001$, $\epsilon_{gb}/\epsilon_{gc}=10$, and a volume fraction of 0.385 for grain cores. See text for code to models

At intermediate values of grain core volume fraction, significant differences between the NCM (or ZBM) and the brick layer models emerge. Figures 8a and b show Z-plane and M-plane plots, respectively, for a conductivity ratio of $\sigma_{gb}/\sigma_{gc}=0.1$ and a dielectric constant ratio of $\epsilon_{gb}/\epsilon_{gc} = 100$ at a grain core volume fraction of 0.385. Similarly, Figures 9a and b show Z-plane and C-Bode plots, respectively, for the same grain core volume fraction (0.385), but with a conductivity ratio of $\sigma_{gb}/\sigma_{gc}=0.001$ and a dielectric constant ratio of $\epsilon_{gb}/\epsilon_{gc} = 10$. In both cases the ratio of grain core-to-grain boundary dimension is $D/d \sim 2.66$ (NCM and SP-BLM). As at smaller grain core volume fraction (e.g., $\phi=0.162$), there is good agreement between the NCM and ZBM predictions; the difference in grain core morphology between the two models does not seem to make a significant difference in their frequency-dependent impedance/dielectric behavior.

The differences between the brick layer model results and the NCM/ZBM predictions are noteworthy. This would support the contention that an EMT-like approach is necessary to account for the true current distributions in the nanostructure, rather than discounting the role of parallel-path grain boundaries (in the S-BLM) or restricting current flow in series vs. parallel paths (in the SP-BLM and SP'-BLM). To test the general validity of the NCM, we calculated the DC conductivity vs. grain core volume fraction over its entire range ($0 < \phi < 1$) for a conductivity ratio of $\sigma_{gb}/\sigma_{gc} = 0.01$ or conversely $\sigma_{gb}/\sigma_{gc} = 10$. This is plotted against the SP-BLM and MW-HS models in Figure 10. (The ZBM and S-BLM were not plotted, since they do not cover the entire volume fraction range.) The MW-HS lines are definitive, since they represent the absolute upper (conductive matrix) and lower bounds (resistive matrix) for isotropic composites. Whereas the SP-BLM results clearly fall outside the allowed range at certain volume fractions, the NCM predictions consistently fall within the allowed range.

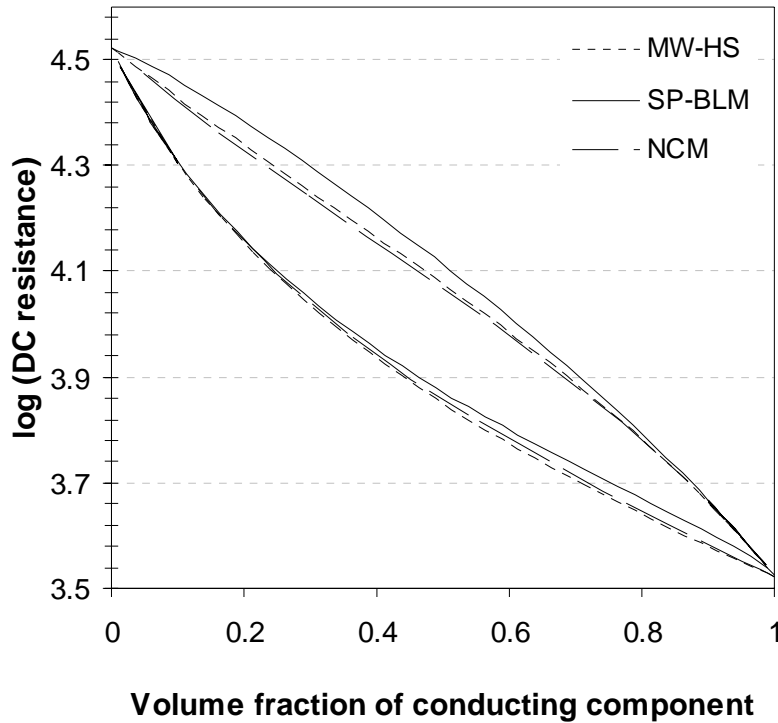


Figure 10. DC resistivity bounds for various models assuming $\sigma_{gb}/\sigma_{gc} = 0.1$ for the upper bound and $\sigma_{gb}/\sigma_{gc} = 10$ for the lower bound. See text for code to models.

The C-Bode plot differences in Figure 9b are also of note. This dual-plateau behavior is characteristic of (RC)(RC) equivalent circuit interpretation (as in Figure 3a). We have shown that the high frequency plateau is given by [23]:

$$C_{re}(hiv) = C_2 C_1 / (C_1 + C_2) \quad (2A)$$

and the low frequency plateau is given by:

$$C_{re}(lov) = (R_2^2 C_2 + R_1^2 C_1) / (R_1 + R_2)^2 \quad (2B)$$

Only in the case of $C_2 \gg C_1$ is $C_{re}(hiv) \approx C_1$, and with the additional constraint that $R_2 \gg R_1$ is $C_{re}(lov) \approx C_2$. This corresponds to the classical BLM instance where the second ($R_2 C_2$) component corresponds to very thin (therefore high capacitance) grain boundaries, usually with a high resistance compared to the grain cores. It follows, however, that if the grain boundaries are neither thin (as in Figure 1) nor much more resistive than the grain cores, the high frequency C-Bode plateau will be a combination of the two component capacitances (Eq. 2A) whereas the low frequency plateau will be a still more complex combination of all four parameters (Eq. 2B). Unfortunately, many impedance/dielectric spectroscopy practitioners are prone to derive the dielectric constant for a given microstructural element directly from what they interpret to be the corresponding C-Bode plateau. This is highly suspect in the nanoscale regime, where the C-

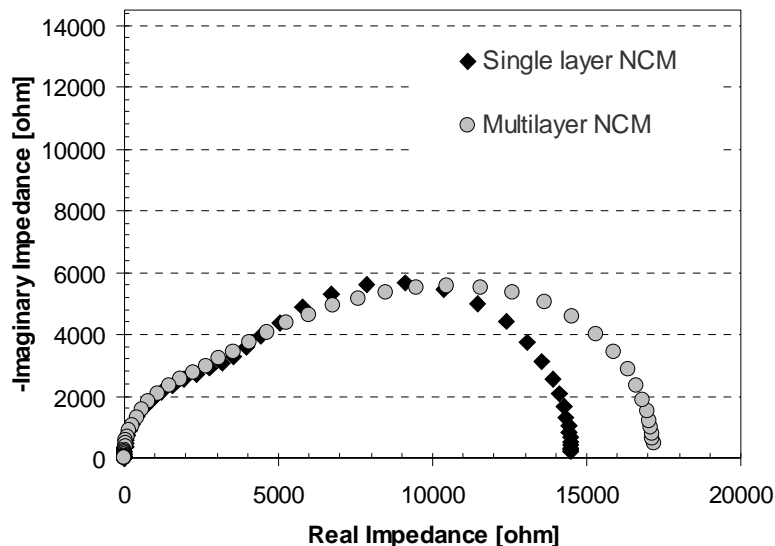


Figure 11. Nested cube model simulations of the impedance response for a single layer vs. a multi-layer grain boundary (simulating spatially varying grain boundary properties). See text for code to models.

Bode plateaus are bound to be complex functions of the four constituent electrical parameters (σ_1 , σ_2 , ϵ_1 , ϵ_2) and the volume fraction of grain cores. The NCM should be much more reliable insofar as fitting impedance/dielectric spectra in the nanoregime in terms of local component electrical properties and volume fractions.

The nested cube approach can be modified to account for multi-layer grain boundaries and/or spatial gradients of electrical properties, e.g., associated with space charge regions. Figure 11 shows preliminary Z-plane simulations for a grain boundary with three layers. Here we have subdivided a grain boundary layer representing 61.5% of the overall grain volume whose values are $\sigma_{gb}/\sigma_{gc}=0.1$ and $\epsilon_{gb}/\epsilon_{gc}=100$ into three layers of equal width (1/3 each) totaling 61.5% of the microstructure, and whose resistivities vary from 150% of the average in the near-grain boundary layer(s) to 100% of the average in the middle layer to 50% of the average in the near-grain core layer. Similarly, the local dielectric constant has been varied in the same manner from layer to layer. This structure is hardly representative of the variation in properties in a space charge region. Nevertheless, it offers some insight into the effect of local property variations on the resulting impedance response. There is noticeable arc-depression for the multilayer NCM as compared to the single layer NCM in Figure 11. Similar arc-depression has been reported for nanoceramics in the literature [23]. Further work in this area is warranted.

CONCLUSIONS

A novel “nested cube model” (NCM) has been developed to describe the frequency-dependent behavior of electroceramics in the nanocrystalline regime. The NCM is capable of

describing behavior over the entire range of grain sizes, from nanocrystalline (where grain core volume fractions are small) to microcrystalline (where grain boundary thicknesses are small). It was shown that the NCM agrees with effective medium theory (Maxwell-Wagner/Hashin-Shtrikman model) at small grain core volume fractions, with the Zuzovsky-Brenner model (grain core spheres on a simple cubic lattice) at intermediate grain core volume fractions, and with the brick layer models at large grain core volume fractions, as expected. In the intermediate volume fraction regime, the NCM is a more accurate model to describe the current distributions between grain cores and grain boundaries. Such a model is necessary to accurately deconvolute local electrical properties (conductivity, dielectric constant) from impedance/dielectric spectra. The NCM can be modified to account for multi-layers and/or spatial property gradients at grain boundaries.

ACKNOWLEDGMENTS

This work was supported in part by the U.S. Department of Energy under grant no. DE-FG02-84ER45097 and in part by the National Science Foundation under grant no. DMR-0076097 through the Materials Research Science and Engineering Center program.

REFERENCES

1. Y.-M. Chiang, , J. Electroceram. **1** (3), 205 (1997).
2. N.J. Dudney, Ann. Rev. Mater. Sci. **19**, 103 (1989).
3. J. Maier, Prog. Solid State Chem. **23**, 171 (1995).
4. J. Maier, Ber. Busenges. Phys. Chem. **90**, 26 (1986).
5. N.M. Beekmans and L. Heyne, Electrochim. Acta **21**, 303 (1976).
6. T. van Dijk and A.J. Burggraaf, Phys. Stat. Solidi A **63**, 229 (1981).
7. M.J. Verkerk, B.J. Middlehuis, and A.J. Burggraaf, Solid State Ionics **6**, 159 (1982).
8. B.A. Boukamp, "Equivalent Circuit (EQUIVCRT.PAS)," University of Twente, The Netherlands (1990).
9. N. Bonanos, B.C.H. Steele, E.P. Butler, W.B. Johnson, W.L. Worrell, D.D. Macdonald, and M.C.H. McKubre, in *Impedance Spectroscopy: Emphasizing Solid Materials and Systems*, edited by J.R. Macdonald, (Wiley and Sons, New York, 1987) pp. 191-205 .
10. H. Näfe, Solid State Ionics **13**, 255 (1984).
11. J.-H. Hwang, D.S. McLachlan, and T.O. Mason, J. Electroceram. **3** (1), 7 (1999).
12. S. Kim and J. Maier, J. Electrochem. Soc., preprint.
13. D.S. McLachlan, J.-H. Hwang, and T.O. Mason, J. Electroceram. **5** (1), 37 (2000).
14. K.M. Wagner, in *Arkiv Electrotechnik*, edited by H. Schering, (Springer-Verlag, Berlin, 1914).
15. J.C. Maxwell, *A Treatise on Electricity and Magnetism*, 2nd ed. (Clarendon Press, Oxford, 1881).
16. Z. Hashin and S. Shtrikman, J. Appl. Phys. **33**, 3125 (1962).
17. J. Fleig and J. Maier, J. Electrochem. Soc. **145**, 2081 (1998).
18. J. Fleig and J. Maier, J. Eur. Ceram. Soc. **19**, 693 (1999).
19. R. Hagenbeck and R. Waser, Ber. Busenges. Phys. Chem. **101**, 1238 (1997).
20. M. Zuzovsky and H. Brenner, J. Appl. Math. Phys. **28**, 979 (1977).

21. E.J. Garboczi, NIST Internal Report **6269** (1998). Also available at <http://ciks.cbt.nist.gov/monograph/>, Chap. 2.
22. J.F. Douglas and E.J. Garboczi, in *Adv. Chem. Phys.*, Vol. XCI, edited by I. Prigogine and S.A. Rice, (Wiley & Sons, 1995), p. 85.
23. T.O. Mason, J.-H. Hwang, N. Mansourian-Hadavi, G.B. Gonzalez, B.J. Ingram, and Z.J. Homrighaus, in *Nanocrystalline Metals and Oxides: Selected Properties and Applications*, edited by P. Kauth and J. Schoonman, (Kluwer Academic Publishers, Norwell, MA, 2002), p. 111.